

A locally modified second-order finite element method for interface problems

Stefan Frei*

Gozel Judakova[†]

Thomas Richter[‡]

The locally modified finite element method, which is introduced in^[1], is a simple fitted finite element method that is able to resolve weak discontinuities in interface problems. The method is based on a fixed structured coarse mesh, which is then refined into sub-elements to resolve an interior interface. In this work, we extend the locally modified finite element method to second order using an isoparametric approach in the interface elements. Thereby we need to take care that the resulting curved edges do not lead to degenerate sub-elements. We prove optimal a priori error estimates in the L^2 -norm and in a modified energy norm, as well as a reduced convergence order of $\mathcal{O}(h^{3/2})$ in the standard H^1 -norm. Finally, we present numerical examples to substantiate the theoretical findings.

Keywords fitted finite elements, interface problem, a priori error estimates, weak discontinuities

1 Introduction

In this paper, we extend the locally modified finite element method introduced in^[1–3] to higher order. We investigate interface problems, where the normal derivative of the solution may have a jump over an interior interface. Such problems arise frequently in environmental engineering in connection with fluid-structure interaction problems and multiphase flows, such as gas-liquid and particle-laden gas flows. For the sake of simplicity, we focus here on the Laplace equation with discontinuous coefficients. We assume that the domain Ω is divided into $\Omega = \Omega_1 \cup \Gamma \cup \Omega_2$ with an interior interface $\Gamma := \partial\Omega_1 \cap \partial\Omega_2$ and a discontinuous coefficient $\nu > 0$ across Γ and consider the equations

$$-\nabla \cdot (\nu_i \nabla u) = f \text{ on } \Omega_i, \quad i = 1, 2, \quad (1)$$

$$[u] = 0, \quad [\nu \partial_n u] = 0, \text{ on } \Gamma, \quad (2)$$

$$u = 0, \text{ on } \partial\Omega, \quad (3)$$

where $\nu|_{\Omega_i} := \nu_i$, $i = 1, 2$.

We denote the jump $[w]$ at the interface Γ with normal vector \mathbf{n} by

$$[w](x) := \lim_{s \searrow 0} w(x + s\mathbf{n}) - \lim_{s \nearrow 0} w(x + s\mathbf{n}) \quad x \in \Gamma.$$

*Department of Mathematics & Statistics, University of Konstanz, Germany (stefan.frei@uni-konstanz.de)

[†]Institut für Analysis und Numerik, University of Magdeburg, Germany, (gozel.judakova@ovgu.de)

[‡]Institut für Analysis und Numerik, University of Magdeburg, Germany (thomas.richter@ovgu.de)

The corresponding variational formulation of the problem (1) is given by

$$u \in H_0^1(\Omega) : \sum_{i=1}^2 (\nu_i \nabla u, \nabla \varphi) = (f, \varphi) \quad \forall \varphi \in H_0^1(\Omega). \quad (4)$$

This interface problem is intensively discussed in the literature. Babuška^[4] shows that a standard finite element ansatz shows low accuracy, regardless of the polynomial degree of the finite element space:

$$\|u - u_h\|_{\Omega} = \mathcal{O}(h), \quad \|\nabla(u - u_h)\|_{\Omega} = \mathcal{O}(h^{1/2}).$$

To improve the accuracy, the interface needs to be resolved within the discretization. Frei and Richter^[1] presented a locally modified finite element method based on first-order polynomials with first-order accuracy in the energy norm and second order in the L^2 -norm. The method is based on a fixed coarse *patch mesh* consisting of quadrilaterals, which is independent of the position of the interface. The patch elements are then divided into sub-elements, such that the interface is locally resolved. The discretization is based on piecewise linear finite elements which has a natural extension to higher order finite element spaces.

The *locally modified finite element method* has been used by the authors and co-workers^[3,5-7], and by Langer & Yang^[8] for fluid-structure interaction (FSI) problems, including the transition between FSI and solid-solid contact^[9,10]. Holm et al.^[11] and Gangl & Langer^[12] used a corresponding approach based on triangular patches, the latter work being motivated by a topology optimisation problem. A pressure stabilization technique for flow problems has been developed in^[13] and a suitable (second-order) time discretisation scheme in^[14]. Due to the fixed coarse patch mesh, which is independent of the interface position, the method is particularly advantageous for problems with moving interfaces and domains, compared to other *fitted* finite element schemes. Details on the implementation in deal.ii and the corresponding source code have been published in^[15,16]. Extensions to three space dimensions have been developed by Langer & Yang^[17], where octahedral coarse cells are divided into sub-elements consisting of octahedra and tetrahedra, and by Höllbacher & Wittum, where a coarse mesh consisting of tetrahedra is sub-divided into hexahedrons, prisms and pyramids^[18,19].

Alternative approaches are unfitted methods, where the mesh is fixed and does not resolve the interface. Prominent examples are the extended finite element method (XFEM^[20]), the generalised finite element (GFEM^[21]) and Cut Finite Elements^[22,23]. For the latter a higher order unfitted finite element method has been developed and analyzed by Lehrenfeld and Reusken (see^[24-26]).

For further *fitted* finite element methods, we refer to^[27-31]. Some works are similar to the *locally modified finite element methods* in the sense that only mesh elements close to the interface are altered^[32,33]. A *fitted* method with higher order approximation has been developed by Fang^[34].

After this introduction, we describe the locally modified high order finite element approach and show a maximum angle condition in Section 2. In Section 3, we derive the main results of this work, namely a priori error estimates in the L^2 -, the H^1 - and in a modified energy norm. Section 4 gives some details on the implementation and in Section 5, we show different numerical examples. The conclusion of our work follows in Section 6.

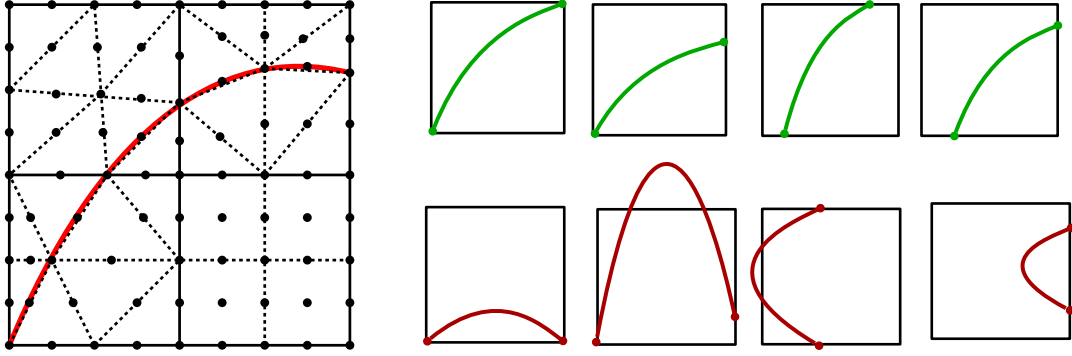


Figure 1. Left: Mesh consisting of four patches, three of which are cut by the interface. Right: possible configurations (top), and configurations that are not allowed (bottom).

2 Locally modified high order finite element method

In this section we review the first order approach proposed by Frei and Richter^[1] and extend it to a second order discretization. The splitting into subelements that we propose is slightly different from the one presented in^[1] and leads in general to a better bound for the maximal angles within the triangles.

Let \mathcal{T}_P be a form and shape-regular quadrilateral mesh of the given domain Ω . We call the elements $P \in \mathcal{T}_P$ the patches and these do not necessarily resolve the partitioning. The interface Γ may cut the patches. In this case we make next assumption:

- Assumption 1.** 1. Each patch $P \in \mathcal{T}_P$ is either cut $P \cap \Gamma \neq \emptyset$ or not cut $P \cap \Gamma = \emptyset$. If it cuts, then it cuts in exactly two points on the boundary, see Figure 1 (left and top right).
2. The interface can not cut the same edge multiple times and may not enter and leave the patch at the same edge, see Figure 1 (bottom right).

The patch mesh \mathcal{T}_P is the fixed background mesh used in the parametric finite element method described below. We will introduce a further local refinement of the mesh, denoted \mathcal{T}_h where the interface is resolved. However, this refined mesh is only for illustrative purpose. The numerical realization is based on the fixed mesh \mathcal{T}_P and the "refinement" is in fact only included in a parametric way within the reference map for each patch $P \in \mathcal{T}_P$.

If the interface is matched by one of the edges of the patch, then the patch is considered as not cut. We will split such patches into four quadrilaterals. If the interface cuts the patch, then the patch splits either in eight triangles or in four quadrilaterals. In both ways, the patch P is first split into four quadrilaterals, which are then possibly refined into two triangles each. This two-step procedure will simplify the following proofs. We define the isoparametric finite element space $V_h \subset H_0^1(\Omega)$

$$V_h := \{\varphi \in C(\Omega) \mid (\varphi \circ T^{-1}) \in \mathcal{P}_K^r(\hat{K}) \text{ for } K \in \mathcal{T}_h\}, \quad (5)$$

where

$$\mathcal{P}_K^r(\hat{K}) := \begin{cases} Q_r(\hat{K}), & K \text{ is a quadrilateral,} \\ P_r(\hat{K}), & K \text{ is a triangle,} \end{cases}$$

and T is a transformation from the reference element \hat{K} to K . The space V_h is continuous, as the restriction of a function in $Q_r(\hat{K})$ to a line $e \subset \partial T$ is in $P_r(\hat{K})$.

2.1 Maximum angle condition

In order to show optimal-order error estimates, the finite element mesh needs to fulfill a maximum angle condition in a fitted finite element method. We first analyse the maximum angles of the subtriangles for a Cartesian patch grid \mathcal{T}_P . A bound for a general regular patch mesh can be obtained by using the regularity of the reference map T .

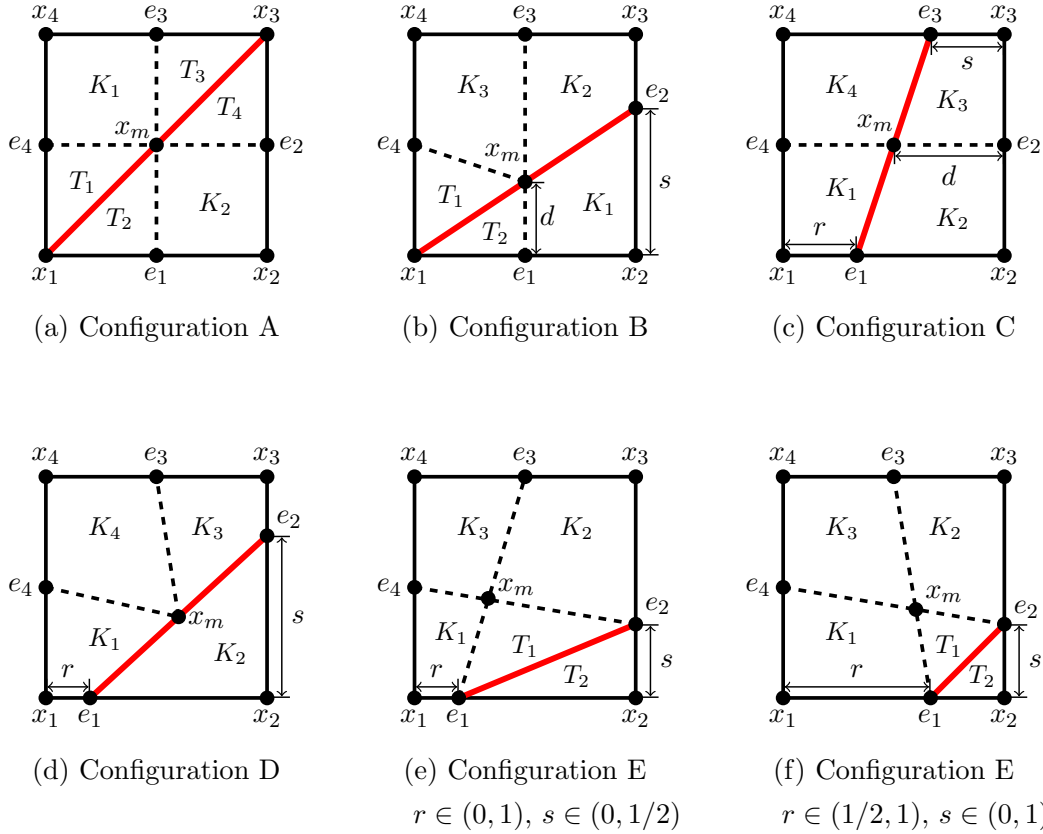


Figure 2. Different configurations and splitting into four large quadrilaterals K_1, \dots, K_4 . The red line shows a linear approximation of the interface. In quadrilaterals that are not split by the interface, we divide in such a way into subtriangles, that the largest angle is split.

Linear interface approximation We distinguish five different types of interface cuts by the fact that the interface intersects a patch either in 1 or 2 exterior vertices (Config. B and A) or two opposite (C) or adjacent (D and E) edges, see Figure 2.

Denoting the relative cut positions on an edge e by $r, s \in (0, 1)$, we distinguish in the case of adjacent edges further between the case that $r \leq \frac{1}{2}$ and $s \geq \frac{1}{2}$ (D) and the case that one of these inequalities is violated (E). In all cases the patch element can be split in four large quadrilaterals K_1, \dots, K_4 first, which are then split into two sub-triangles, if the interface cuts through the patch. Details are given in the appendix.

Considering arbitrary interface positions, anisotropic elements can arise, when the relative cut position $r, s \in (0, 1)$ on an edge e tends to 0 or 1 (see Figure 2). We can not guarantee a minimum angle condition for the sub-triangles, but we can ensure that the maximum angles remain bounded away from 180° .

Lemma 1 (Linear approximation of the interface). *All interior angles of the Cartesian patch elements shown in Figure 2 are bounded by 135° independently of the parameters $r, s \in (0, 1)$.*

Proof. The proof follows by basic geometrical considerations, see Appendix B. \square

Theorem 2. *We assume that the patch grid \mathcal{T}_P is Cartesian. For all types of the interface cuts (see Figure 2), the interior angles of all subelements are bounded by 135° independently of the parameters $r, s \in (0, 1)$.*

Proof. By means of Lemma 1 all interior angles on the reference patch are bounded by 135° . As all cells are Cartesian, the same bound holds for the elements $T \in \mathcal{T}_P$. \square

Remark 1. *We have assumed for simplicity that the underlying patch mesh is fully Cartesian. This assumption can, however, easily be weakened. Allowing more general form- and shape-regular patch meshes a geometric transformation of each patch to the unit patch will give a bound $\alpha < \alpha_{\max} < 180^\circ$ for the interior angles α (with α_{\max} larger than 135°).*

Quadratic interface approximation Next, we define a quadratic approximation of the interface. In each of the subtriangles obtained in the previous paragraph, we consider 6 degrees of freedom that lie on the vertices and edge midpoints of the triangles (see the dots in Figure 1, left). In order to guarantee a higher-order interface approximation those that lie on the discrete interface Γ_h need to be moved. The detailed algorithm is given in Section 4.

In certain “pathological” situations we can not guarantee that the angle conditions imposed above are fulfilled. This is due to the fact that the curved edges that correspond to a quadratic interface approximation might intersect other edges, see Figure 3 for an example.

In this case, we use a linear approximation of the interface in the affected patch. We will see in the numerical examples below that this happens rarely. Moreover, it is reasonable to assume that the maximum number of such patches remains bounded under refinement independently of $h \leq h_0$. To show a priori error bounds in Section 3 we will assume that the interface allows for a C^3 -parametrization. Hence, the curvature of the interface is bounded which makes sure that the interface, in relation to the surrounding patch, will converge to a straight line if $\text{diam}(P) \rightarrow 0$. We will denote the maximum number of patches with a linear interface approximation by n_l .

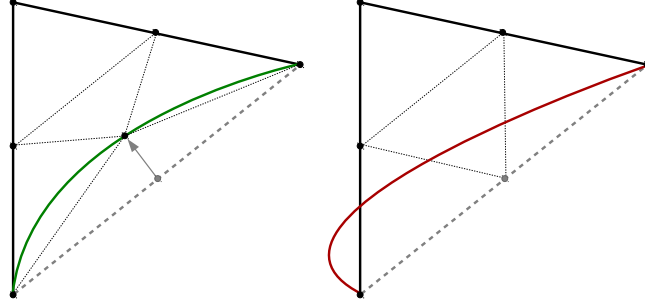


Figure 3. Triangle with a curved edge. *Left:* We can move the edge midpoint to the interface. *Right:* A fully quadratic interface approximation would result in a degenerate element.

2.2 Modified spaces and discrete variational formulation

We use the space V_h defined in (5)

$$V_h := \{\varphi \in C(\Omega) \mid (\varphi \circ T^{-1}) \in \mathcal{P}_K^r(\hat{K}) \text{ for } K \in \mathcal{T}_h\}, \quad (6)$$

where the map T resolves the interface with order r in all but n_l elements, where the approximation is only linear. The polynomial order of the trial functions $\varphi \circ T^{-1}$ is r independent of the interface approximation.

We consider a C^3 -parameterized interface Γ , which is not matched by the triangulation \mathcal{T}_h . The triangulation induces a discrete interface Γ_h , which is a quadratic (and in max. n_l elements a linear) approximation to Γ . The discrete interface splits the triangulation in subdomains Ω_h^1 and Ω_h^2 , such that each subtriangle $K \in \mathcal{T}_h$ is either completely included in Ω_h^1 or in Ω_h^2 .

We consider the following discrete variational formulation: *Find $u_h \in V_h$ such that*

$$a_h(u_h, \phi_h) = (f_h, \phi_h)_\Omega \quad \forall \phi_h \in V_h, \quad (7)$$

where we set $f_h|_{\Omega_h^i} := f_i, i = 1, 2$ and f_i is a smooth extension of $f|_{\Omega_i}$ to Ω_h^i . The bilinear form is given by

$$a_h(u_h, \phi_h) := (\nu_h \nabla u_h, \nabla \phi_h)_\Omega,$$

where ν_h is defined by

$$\nu_h = \begin{cases} \nu_1, & x \in \Omega_h^1 \\ \nu_2, & x \in \Omega_h^2. \end{cases}$$

3 A priori error analysis

Let h_P be the maximum size of a patch element $P \in \mathcal{T}_P$ of the regular patch grid. We will denote the mismatch (see Figure 4) between Ω_h^i and Ω^i by $S_h^i, i = 1, 2$

$$\begin{aligned} S_h^1 &:= \Omega_h^1 \setminus \Omega_1 = \Omega_2 \setminus \Omega_h^2, \\ S_h^2 &:= \Omega_h^2 \setminus \Omega_2 = \Omega_1 \setminus \Omega_h^1. \end{aligned}$$

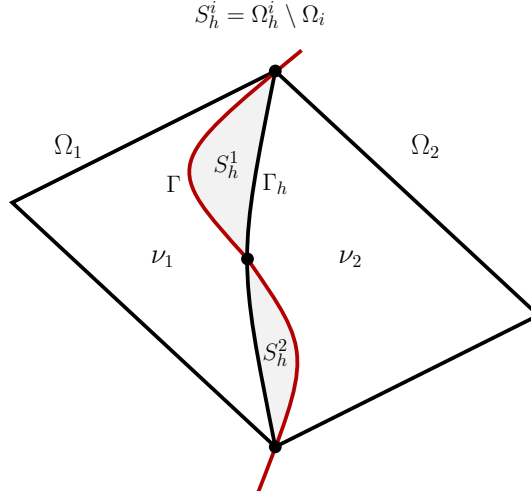


Figure 4. Mismatch between Ω^i and Ω_h^i , $i = 1, 2$ at two elements along the curved interface.

Moreover, we denote the set of elements $T \in \mathcal{T}_h$ that contain parts of S_h^i by

$$S_T^i := \{T \in \mathcal{T}_h \mid T \cap S_h^i \neq \emptyset\}, \quad S_T := S_T^1 \cup S_T^2.$$

Further, we split S_h^i into parts $S_{h,\text{lin}}^i$ with a linear approximation of the interface and parts $S_{h,\text{qu}}^i$ with a quadratic approximation. Finally, by a slight abuse of notation, we will use the same notation, e.g. S_T, S_T^i , for the region that is spanned by the union of the triangles in these sets.

3.1 Auxiliary estimates

We begin with some technical estimates that will be needed in order to control the mismatch between continuous and discrete bilinear forms.

Lemma 3 (Geometry Approximation). *Let $T \in S_T$ and let s be the local approximation order of the interface, i.e.*

$$\text{dist}(\Gamma_h \cap T; \Gamma \cap T) \leq ch_P^{s+1}. \quad (8)$$

If the number of elements with a linear interface approximation is bounded by n_l , it holds for the areas of the regions $S_{h,\text{lin}}$ and $S_{h,\text{qu}}$ that

$$|S_{h,\text{lin}}| \leq n_l h_P^3, \quad |S_{h,\text{qu}}| \leq h_P^3. \quad (9)$$

For $u \in H^1(\Omega_1 \cup \Omega_2)$ and $\phi_h \in \mathcal{V}_h$ we have the bounds

$$\|\nabla \phi_h\|_{S_h \cap T} \leq ch_P^{\frac{s}{2}} \|\nabla \phi_h\|_T \quad (10)$$

$$\|u\|_{S_h \cap T} \leq ch_P^{\frac{s+1}{2}} \|u\|_{\Gamma \cap T} + ch_P^{s+1} \|\nabla u\|_{S_h \cap T}. \quad (11)$$

Moreover, we have for $u \in H^1(\Omega_1 \cup \Omega_2)$ and $v \in H^2(\Omega_1 \cup \Omega_2)$

$$\|u\|_{S_{h,\text{lin}}} \leq ch_P \|u\|_{H^1(\Omega_1 \cup \Omega_2)}, \quad \|u\|_{S_{h,\text{qu}}} \leq ch_P^{\frac{3}{2}} \|u\|_{H^1(\Omega_1 \cup \Omega_2)} \quad (12)$$

and for an arbitrary $\epsilon > 0$

$$\|u\|_{S_{h,lin}} \leq c(\epsilon) n_l^{\frac{1}{2}} h_P^{\frac{3}{2}-\epsilon} \|u\|_{H^1(\Omega_1 \cup \Omega_2)}, \quad \|v\|_{S_{h,lin}} \leq c n_l^{\frac{1}{2}} h_P^{\frac{3}{2}} \|v\|_{H^2(\Omega_1 \cup \Omega_2)}, \quad (13)$$

where $c(\epsilon) \rightarrow \infty$ for $\epsilon \rightarrow 0$. For functions $u \in H_0^1(\Omega)$ the H^1 -norm on the right-hand side of (12) and (13) can be replaced by the H^1 -seminorm.

Proof. Estimates (9)-(11) have been shown in [2]. (9) follows from (8) and simple geometric arguments. For (10) and (11) a Poincaré-type estimate is used, see [2, Lemma 4.34]

$$\|u\|_{S_h \cap T}^2 \leq c h_P^{s+1} \|u\|_{\Gamma_h \cap T}^2 + c h_P^{2s+2} \|\nabla u\|_{S_h \cap T}^2. \quad (14)$$

Summation over all elements in $S_{T,lin}$ and $S_{T,qu}$, respectively, and a global trace inequality for the interface terms yields (12). To show (13), we use a Hölder inequality for $p \in [2, \infty)$

$$\|u\|_{S_{h,lin}} \leq |S_{h,lin}|^{\frac{1}{2}-\frac{1}{p}} \|u\|_{L^p(S_{h,lin})}. \quad (15)$$

Due to the Sobolev imbedding $H^1(\Omega_i) \subset L^p(\Omega_i)$ for $p < \infty$ and $|S_{h,lin}| \leq c n_l h_P^3$, we have

$$\|u\|_{S_{h,lin}} \leq c(\epsilon) n_l^{\frac{1}{2}} h_P^{\frac{3}{2}-\epsilon} \|u\|_{H^1(\Omega_1 \cup \Omega_2)}, \quad (16)$$

where $c(\epsilon) \rightarrow \infty$ for $\epsilon \rightarrow 0$. If $v \in H^2(\Omega_1 \cup \Omega_2)$ we can use (15) for $p = \infty$ due to the Sobolev imbedding $H^2(\Omega_i) \subset L^\infty(\Omega_i)$ and we obtain

$$\|u\|_{S_{h,lin}} \leq c n_l^{\frac{1}{2}} h_P^{\frac{3}{2}} \|u\|_{H^2(\Omega_1 \cup \Omega_2)}. \quad (17)$$

Finally, the norms on the right-hand side can be substituted by the H^1 -seminorm for $u \in H_0^1(\Omega)$ by means of the Poincaré inequality. \square

In the following estimates the mismatch between discrete and continuous bilinear form will be the predominant issue and will lead to some technicalities in the estimates. The continuous solution u is regular in Ω_1 and Ω_2 , while its normal derivative has a jump across Γ . Discrete functions can only have irregularities at the boundaries of cells ∂T , which means that at best a discrete function can resemble a similar discontinuity across the discrete interface Γ_h .

To cope with this difference, we will need a map $\pi : H^3(\Omega_1 \cup \Omega_2) \rightarrow H^3(\Omega_h^1 \cup \Omega_h^2)$. To define the map, let $u \in H^3(\Omega_1 \cup \Omega_2)$ and $u_i := u|_{\Omega_i} \in H^3(\Omega_i)$ the restriction to the subdomain Ω_i , $i = 1, 2$. We use smooth extensions $\tilde{u}_i \in H^3(\Omega)$ ($i=1,2$) to the full domain Ω . Such an extension with the properties

$$\|\tilde{u}_i - u\|_{H^m(\Omega_i)} = 0, \quad \|\tilde{u}_i\|_{H^m(\Omega)} \leq C \|u\|_{H^m(\Omega_i)}, \quad i = 1, 2, \quad m = 2, 3, \quad (18)$$

exists, as the interface Γ is smooth, see e.g. the textbook of Wloka [35]. We use these extensions to define a function $\pi u \in H^3(\Omega_h^1 \cup \Omega_h^2)$:

$$\pi u = \begin{cases} \tilde{u}_1, & x \in \Omega_h^1, \\ \tilde{u}_2, & x \in \Omega_h^2. \end{cases} \quad (19)$$

It should be noted that πu can be discontinuous across Γ_h .

The following estimate analyzes the difference between u and πu in the H^1 -seminorm.

Lemma 4. *Let $u \in H^3(\Omega_1 \cup \Omega_2)$, $\pi u \in H^3(\Omega_h^1 \cup \Omega_h^2)$ the function defined by (19) and n_l the maximum number of elements with a linear interface approximation. It holds that*

$$\|\nabla(u - \pi u)\|_\Omega \leq ch_P \left(n_l^{1/2} + 1 \right) \|u\|_{H^2(\Omega_1 \cup \Omega_2)} \quad (20)$$

$$\|\nabla(u - \pi u)\|_\Omega \leq ch_P^{3/2} \left(n_l^{1/2} + 1 \right) \|u\|_{H^3(\Omega_1 \cup \Omega_2)}. \quad (21)$$

Proof. u and πu differ only in the small strip S_h around the interface. For $u \in H^3(\Omega_i)$ we have, using the Sobolev embedding $H^3(\Omega_i) \subset W^{1,\infty}(\Omega_i)$ and the continuity of the extensions (18)

$$\begin{aligned} \|\nabla(u - \pi u)\|_\Omega &= \|\nabla(u - \pi u)\|_{S_h} \leq |S_h|^{\frac{1}{2}} (\|\nabla u\|_{L^\infty(\Omega)} + \|\nabla \pi u\|_{L^\infty(\Omega)}) \\ &\leq c|S_h|^{\frac{1}{2}} \|u\|_{H^3(\Omega_1 \cup \Omega_2)}. \end{aligned}$$

(21) follows by means of (9).

To show (20), we note that $u - \pi u$ vanishes in cells $T \in \mathcal{T}_h \setminus S_T$. Thus, let $T \in S_T$ and let $s \in \{1, 2\}$ be the local approximation order of the interface in T . We use (11) and the fact that $s \geq 1$ to get

$$\begin{aligned} \|\nabla(u - \pi u)\|_T &= \|\nabla(u - \pi u)\|_{S_h \cap T} \leq ch_P^{\frac{1+s}{2}} \|\nabla(u - \pi u)\|_{\Gamma \cap T} + ch_P^{1+s} \|\nabla^2(u - \pi u)\|_{S_h \cap T} \\ &\leq ch_P (\|\nabla u\|_{\Gamma \cap T} + \|\nabla \pi u\|_{\Gamma \cap T}) + ch_P^2 (\|\nabla^2 u\|_{S_h \cap T} + \|\nabla^2 \pi u\|_{S_h \cap T}), \end{aligned}$$

where the derivatives on Γ need to be seen from S_h .

After summation over all cells $T \in \mathcal{T}_h$ a global trace inequality and the continuity of the extension (18) yield

$$\|\nabla(u - \pi u)\|_\Omega \leq ch_P (\|u\|_{H^2(\Omega_1 \cup \Omega_2)} + \|\pi u\|_{H^2(\Omega_1 \cup \Omega_2)}) \leq ch_P \|u\|_{H^2(\Omega_1 \cup \Omega_2)}.$$

□

Remark 2. *The estimate (21) is optimal for the difference between functions $u \in H^3(\Omega_1 \cup \Omega_2)$ and functions $v \in H^3(\Omega_h^1 \cup \Omega_h^2)$, that are discontinuous over Γ and Γ_h , respectively. To illustrate this, consider a function u with piecewise constant derivative $\nabla u|_{\Omega_i} = \nabla u_i$ for $i = 1, 2$. For sufficiently small h , the best approximation v in $H^3(\Omega_h^1 \cup \Omega_h^2)$ will have derivatives $\nabla v|_{\Omega_h^i} \approx \nabla u_i$ for $i = 1, 2$. If $\nabla u_1 \neq \nabla u_2$, the difference in the strip S_h with $|S_h| = \mathcal{O}(h_P^{3/2})$ is of order $\mathcal{O}(1)$ and the estimate (21) results as an equality.*

3.2 Interpolation

In this section, we will derive interpolation estimates for a Lagrangian interpolant I_h . In the case of a linear interface approximation, it can happen that some of the Lagrange points lie on Γ_h , but not on Γ . This means that there are elements with Lagrange points $x_i \in \mathcal{L}_T$, that lie in different subdomains Ω_1 and Ω_2 , see Figure 5. Defining the interpolant as $I_h u = \sum_{i \in \mathcal{L}_T} u(x_i)$ would lead to a poor approximation order ($\mathcal{O}(h_P)$ in the H^1 -norm), due to the discontinuity of ∇u across Γ . Each such point x_i lies, however, on a line between two points x_1^* and x_2^* on Γ . We use a linear interpolation of the values $u(x_1^*)$ and $u(x_2^*)$ in order to define $I_h u(x_i) := \frac{1}{2}(u(x_1^*) + u(x_2^*))$, see also^[3] and Fig. 5.

We have the following approximation properties for this modified Lagrangian interpolant.

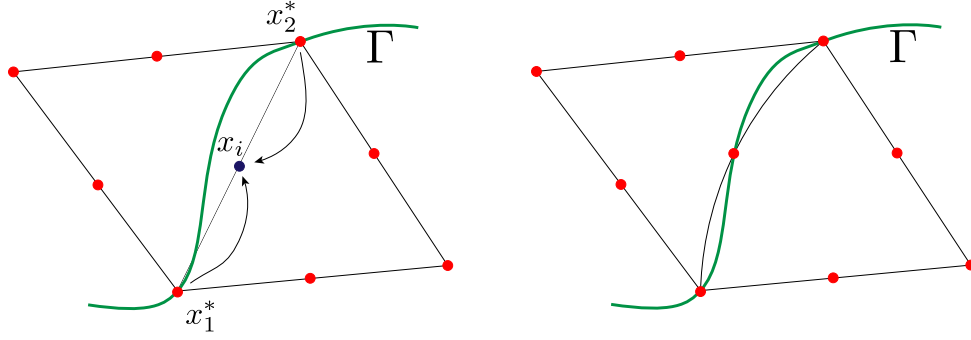


Figure 5. Interpolation operator at the interface. If the interface is approximated with second order (right) we use the standard nodal interpolation. For linear interface approximations (left) we replace the node in the middle of the interface edge by the mean of the two adjacent corner nodes.

Lemma 5 (Interpolation). *Let $u \in \mathcal{U} := [H_0^1(\Omega) \cap H^3(\Omega_1 \cup \Omega_2)]$ and $\tilde{u} = \pi u \in H^3(\Omega_h^1 \cup \Omega_h^2)$ the function resulting from the map π defined in (19). Moreover, we assume that Γ is a smooth interface with C^3 -parametrization and that the interface is approximated with second order in all elements $T \in \mathcal{T}_h$, except for maximum n_l elements, where the interface approximation is linear. It holds for the Lagrangian interpolation operator $I_h : \mathcal{U} \rightarrow V_h$ and an arbitrary $\epsilon > 0$ that*

$$\|\nabla^m(u - I_h u)\|_\Omega \leq ch_P^{2-m} \|u\|_{H^2(\Omega_1 \cup \Omega_2)}, \quad m = 1, 2 \quad (22)$$

$$\|\nabla(u - I_h u)\|_\Omega \leq c \left(n_l^{1/2} + 1 \right) h_P^{3/2} \|u\|_{H^3(\Omega_1 \cup \Omega_2)}, \quad (23)$$

$$\|\nabla(\tilde{u} - I_h u)\|_\Omega \leq (c(\epsilon) n_l^{1/2} h_P^{2-\epsilon} + c_2 h_P^2) \|u\|_{H^3(\Omega_1 \cup \Omega_2)}. \quad (24)$$

with $c(\epsilon) \rightarrow \infty$ for $\epsilon \rightarrow 0$.

Proof. First, we note that it holds $I_h u = I_h \tilde{u}$ by construction of the interpolant, as $u(x_i) = \tilde{u}(x_i)$ in all Lagrange points, that are used in the definition of the interpolant I_h .

Next, we note that the proof of all estimates is standard in all elements $T \in \mathcal{T}_h \setminus S_T$ that are not affected by the interface, since $\tilde{u}|_T = u|_T$, $u \in H^3(T)$ and

$$\|\nabla^m(u - I_h u)\|_T \leq ch_P^{2-m} \|u\|_{H^2(T)} \quad (m = 1, 2), \quad \|\nabla(u - I_h u)\|_T \leq ch_P^2 \|u\|_{H^3(T)}. \quad (25)$$

In elements $T \in S_{T,qu}$ there are no Lagrange points on $\Gamma_h \setminus \Gamma$ and I_h is the standard Lagrangian interpolant. As \tilde{u} is smooth in T , estimate (24) is also standard in elements $T \in S_{T,qu}$

$$\|\nabla(\tilde{u} - I_h u)\|_T = \|\nabla(\tilde{u} - I_h \tilde{u})\|_T \leq ch_P^2 \|\tilde{u}\|_{H^3(T)}.$$

In elements $T \in S_{T,lin}$ the interpolation is only linear due to the modification described above. Let $T \in S_{T,lin}^i$ with $i \in \{1, 2\}$ and let P be the patch that contains T . The following estimate has been shown in [3]

$$\|\nabla(\tilde{u} - I_h u)\|_T = \|\nabla(\tilde{u} - I_h \tilde{u})\|_T \leq ch_P \|\nabla^2 \tilde{u}_i\|_P, \quad (26)$$

where \tilde{u}_i denotes the extension of u_i to Ω . We sum over all elements $T \in S_{T,lin}^i$ and denote by $S_{P,lin}^i$ the region, which is spanned by the patches P containing elements $T \in S_{T,lin}^i$. It holds $|S_{P,lin}^i| = n_l \mathcal{O}(h_P^2)$ and we can estimate further by using the Sobolev imbedding $H^3(\Omega_i) \subset W^{2,p}(\Omega_i)$ for $p < \infty$

$$\begin{aligned} \|\nabla(\tilde{u} - I_h u)\|_{S_{T,lin}^i} &\leq ch_P \|\nabla^2 \tilde{u}_i\|_{S_{P,lin}^i} \\ &\leq ch_P |S_{P,lin}^i|^{\frac{1}{2} - \frac{1}{p}} \|\tilde{u}_i\|_{W^{2,p}(\Omega_i)} \leq c(\epsilon) n_l^{1/2} h_P^{2-\epsilon} \|u\|_{H^3(\Omega_i)} \end{aligned}$$

with $c(\epsilon) \rightarrow \infty$ for $\epsilon \rightarrow 0$. This completes the proof of (24). To show (22) and (23) in elements $T \in S_T$, we split into

$$\|\nabla^m(u - I_h u)\|_T \leq \|\nabla^m(u - \tilde{u})\|_T + \|\nabla^m(\tilde{u} - I_h \tilde{u})\|_T. \quad (27)$$

For $m = 1$, the first term has been estimated in Lemma 4, for $m = 2$ we can use the stability of the extension (18). (23) results from the estimate (24) for the second term. To show (22), we use (26) and standard interpolation estimates. \square

Remark 3. (Optimality of the interpolation estimate) The interpolation estimate (23), i.e.,

$$\|\nabla(u - I_h u)\|_\Omega \leq ch_P^{3/2} \|u\|_{H^3(\Omega_1 \cup \Omega_2)}$$

is optimal even for a fully quadratic interface approximation and can not be improved by using a different interpolation operator. This is due to the mismatch between discrete and continuous interface and the discontinuity of ∇u across it. As $I_h u$ can not resemble this behaviour any better than being discontinuous across Γ_h , an error of order $\mathcal{O}(1)$ results in the small strip S_h which sums up to $\mathcal{O}(h_P^{3/2})$, see Remark 2. In the proof of Lemma 5 this can be seen from the dominant error contribution $\|\nabla(u - \tilde{u})\|_\Omega$ in (27).

3.3 A priori error estimate

We are now ready to prove the main result of this section.

Theorem 6 (A priori estimate). Let $\Omega \subset \mathbb{R}^2$ be a convex domain with polygonal boundary, which is resolved (exactly) by the triangulations \mathcal{T}_h . We assume $f \in H^1(\Omega_1 \cup \Omega_2)$ and a splitting $\Omega = \Omega_1 \cup \Gamma \cup \Omega_2$, where Γ is a smooth interface with C^3 -parametrization that divides the domain in such a way that the solution $u \in H_0^1(\Omega)$ to (4) satisfies the stability estimate $u \in H_0^1(\Omega) \cap H^3(\Omega_1 \cup \Omega_2)$

$$\|u\|_{H_0^1(\Omega)} + \|u\|_{H^3(\Omega_1 \cup \Omega_2)} \leq c_s \|f\|_{H^1(\Omega_1 \cup \Omega_2)}. \quad (28)$$

Moreover, we denote by $\tilde{u} = \pi u \in H^3(\Omega_h^1 \cup \Omega_h^2)$ the map defined in (21) and by n_l the maximum number of elements $K \in \mathcal{T}_h$, where the interface is approximated linearly. For the modified finite element solution $u_h \in V_h$ to (7) it holds for an arbitrary $\epsilon > 0$

$$\|\nu_h^{1/2} \nabla(u - u_h)\|_\Omega \leq c \left(n_l^{\frac{1}{2}} + 1 \right) h_P^{\frac{3}{2}} \|f\|_{H^1(\Omega_1 \cup \Omega_2)}, \quad (29)$$

$$\|\nu_h^{1/2} \nabla(\tilde{u} - u_h)\|_\Omega \leq \left(c(\epsilon) n_l^{\frac{1}{2}} h_P^{2-\epsilon} + c_2 h_P^2 \right) \|f\|_{H^1(\Omega_1 \cup \Omega_2)}, \quad (30)$$

$$\|u - u_h\|_\Omega \leq \left(c(\epsilon) n_l h_P^{3-\epsilon} + c_2 h_P^3 \right) \|f\|_{H^1(\Omega_1 \cup \Omega_2)}, \quad (31)$$

where $c(\epsilon) \rightarrow \infty$ for $\epsilon \rightarrow 0$.

Proof. (i) First, we have the following perturbed Galerkin orthogonality by subtracting (7) from (4)

$$a(u, \phi_h) - a_h(u_h, \phi_h) = (f - f_h, \phi_h)_\Omega \quad \forall \phi_h \in V_h. \quad (32)$$

We start by estimating the right-hand side in (32). The difference $f - f_h$ vanishes everywhere besides on S_h . We have

$$(f - f_h, \phi_h)_\Omega = (f - f_h, \phi_h)_{S_h} \leq (\|f_1\|_{S_h} + \|f_2\|_{S_h}) \|\phi_h\|_{S_h},$$

where f_i denotes a smooth extension of $f|_{\Omega_i}$ to Ω , $i = 1, 2$.

We split the region S_h into parts with a quadratic interface approximation $S_{h,qu}$ and parts with a linear approximation. (12) and (13) yield

$$\begin{aligned} \|f_i\|_{S_{h,qu}} + \|f_i\|_{S_{h,lin}} &\leq ch_P \|f\|_{H^1(\Omega_1 \cup \Omega_2)} \text{ or} \\ \|f_i\|_{S_{h,qu}} + \|f_i\|_{S_{h,lin}} &\leq \left(ch_P^{\frac{3}{2}} + c(\epsilon) n_l^{\frac{1}{2}} h_P^{\frac{3}{2}-\epsilon} \right) \|f\|_{H^1(\Omega_1 \cup \Omega_2)}, \end{aligned} \quad (33)$$

depending on whether we need the full approximation order. The second estimate yields

$$(f - f_h, \phi_h)_\Omega \leq c(\epsilon) \left(h_P^{\frac{3}{2}} + n_l^{\frac{1}{2}} h_P^{\frac{3}{2}-\epsilon} \right) \|f\|_{H^1(\Omega_1 \cup \Omega_2)} \|\phi_h\|_{S_h}, \quad (34)$$

where $c(\epsilon) \rightarrow \infty$ for $\epsilon \rightarrow 0$ if $n_l > 0$.

(ii) Concerning the energy norm estimates (29) and (30), it suffices to show (30). Then, (29) follows by combining (30) and (21). We start by splitting into interpolatory and discrete part

$$\|\nu_h^{1/2} \nabla(\tilde{u} - u_h)\|_\Omega \leq \|\nu_h^{1/2} \nabla(\tilde{u} - I_h u)\|_\Omega + \|\nu_h^{1/2} \nabla(I_h u - u_h)\|_\Omega. \quad (35)$$

The interpolatory part has already been estimated in Lemma 5. For the second term in (35), we use the perturbed Galerkin orthogonality (32) with $\varphi_h := I_h u - u_h$

$$\begin{aligned} \|\nu_h^{1/2} \nabla(I_h u - u_h)\|_\Omega^2 &= (\nu_h \nabla(I_h u - u_h), \nabla(I_h u - u_h))_\Omega \\ &= (\nu_h \nabla I_h u - \nu \nabla u, \nabla(I_h u - u_h))_\Omega + (f - f_h, I_h u - u_h)_\Omega. \end{aligned} \quad (36)$$

We split the first part in (36) further

$$\begin{aligned} (\nu_h \nabla I_h u - \nu \nabla u, \nabla(I_h u - u_h))_\Omega &= (\nu_h \nabla(I_h u - \tilde{u}), \nabla(I_h u - u_h))_\Omega \\ &\quad + (\nu_h \nabla \tilde{u} - \nu \nabla u, \nabla(I_h u - u_h))_\Omega. \end{aligned} \quad (37)$$

For the first part, we use (24) to get

$$(\nu_h \nabla(I_h u - \tilde{u}), \nabla(I_h u - u_h))_\Omega \leq c(\epsilon) \left(n_l^{\frac{1}{2}} + 1 \right) h_P^{2-\epsilon} \|u\|_{H^3(\Omega_1 \cup \Omega_2)} \|\nu_h^{1/2} \nabla(I_h u - u_h)\|_\Omega.$$

The integrand in the second term on the right-hand side of (37) vanishes everywhere besides on S_h . We obtain using the Sobolev imbedding $H^3(\Omega_i) \subset W^{1,\infty}(\Omega_i)$, the continuity of the extension (18) and Lemma 3 ((10) and (9))

$$\begin{aligned} (\nu_h \nabla \tilde{u} - \nu \nabla u, \nabla(I_h u - u_h))_\Omega &= (\nu_h \nabla \tilde{u} - \nu \nabla u, \nabla(I_h u - u_h))_{S_h} \\ &\leq c \left(\|\nabla \tilde{u}\|_{S_h} + \|\nabla u\|_{S_h} \right) \|\nu_h^{1/2} \nabla(I_h u - u_h)\|_{S_h} \\ &\leq c |S_h|^{1/2} \|u\|_{H^3(\Omega_1 \cup \Omega_2)} h_P^{1/2} \|\nu_h^{1/2} \nabla(I_h u - u_h)\|_{S_T} \\ &\leq ch_P^2 \left(n_l^{1/2} + 1 \right) \|u\|_{H^3(\Omega_1 \cup \Omega_2)} \|\nu_h^{1/2} \nabla(I_h u - u_h)\|_\Omega \end{aligned} \quad (38)$$

For the second term in (36), we use (33) and (12)

$$\begin{aligned} (f - f_h, I_h u - u_h)_\Omega &\leq ch_P \|f\|_{H^1(\Omega_1 \cup \Omega_2)} \|I_h u - u_h\|_{S_h} \\ &\leq ch_P^2 \|f\|_{H^1(\Omega_1 \cup \Omega_2)} \|\nu_h^{1/2} \nabla(I_h u - u_h)\|_{\Omega_1 \cup \Omega_2}. \end{aligned}$$

Combining the estimates, we obtain using the stability estimate (28)

$$\|\nu_h^{1/2} \nabla(I_h u - u_h)\|_{\Omega_1 \cup \Omega_2} \leq ch_P^2 \|f\|_{H^1(\Omega_1 \cup \Omega_2)}$$

This completes the proof of the energy estimates.

(iii) To estimate the L^2 - norm error, we define the following adjoint problem. Let $z \in H_0^1(\Omega)$ be the solution of

$$(\nu \nabla \varphi, \nabla z) = \|e_h\|^{-1} (e_h, \varphi)_\Omega \quad \forall \varphi \in H_0^1(\Omega).$$

The solution z lies in $H_0^1(\Omega) \cap H^2(\Omega_1 \cup \Omega_2)$ and satisfies

$$\|z\|_{H^2(\Omega_1 \cup \Omega_2)} \leq c_s.$$

By choosing $\varphi = u - u_h = e_h$ and adding and subtracting $\nu_h \nabla u_h$, we have

$$\|e_h\| = (\nu \nabla e_h, \nabla z)_\Omega = (\nu \nabla u - \nu_h \nabla u_h, \nabla z)_\Omega + ((\nu_h - \nu) \nabla u_h, \nabla z)_\Omega. \quad (39)$$

For the second term in (39), we have

$$((\nu_h - \nu) \nabla u_h, \nabla z)_\Omega = ((\nu_h - \nu) \nabla u_h, \nabla z)_{S_h} \leq C (\|\nu_h \nabla u_h\|_{S_h} \|\nabla z\|_{S_h}) \quad (40)$$

We split the first term on the right-hand side further and use the bound for the energy norm error as well as (13) (Lemma 3)

$$\begin{aligned} \|\nu_h \nabla u_h\|_{S_h} &\leq \|\nu_h \nabla(u_h - u)\|_{S_h} + \|\nu \nabla u\|_{S_h} \\ &\leq c \left(n_l^{\frac{1}{2}} + 1 \right) h_P^{3/2} \|u\|_{H^3(\Omega_1 \cup \Omega_2)}. \end{aligned}$$

For the last term in (40), we obtain from (12) and (13)

$$\begin{aligned} \|\nabla z\|_{S_{h,lin}} &\leq c(\epsilon) n_l^{\frac{1}{2}} h_P^{\frac{3}{2}-\epsilon} \|z\|_{H^2(\Omega_1 \cup \Omega_2)} \leq c(\epsilon) n_l^{\frac{1}{2}} h_P^{\frac{3}{2}-\epsilon}, \\ \|\nabla z\|_{S_{h,qu}} &\leq ch_P^{\frac{3}{2}} \|z\|_{H^2(\Omega_1 \cup \Omega_2)} \leq ch_P^{\frac{3}{2}}. \end{aligned}$$

We conclude for the second term in (39) that

$$((\nu_h - \nu) \nabla u_h, \nabla z)_\Omega \leq c (n_l h_P^{3-\epsilon} + h_P^3) \|u\|_{H^3(\Omega_1 \cup \Omega_2)}. \quad (41)$$

For the first term in (39), we add and subtract the interpolant $\nabla I_h z$, as well as $\pm \nu_h \tilde{u}$

$$\begin{aligned} (\nu \nabla u - \nu_h \nabla u_h, \nabla z)_\Omega &= (\nu \nabla u - \nu_h \nabla \tilde{u}, \nabla(z - I_h z))_\Omega + (\nu_h \nabla(\tilde{u} - u_h), \nabla(z - I_h z))_\Omega \\ &\quad + (\nu \nabla u - \nu_h \nabla u_h, \nabla I_h z)_\Omega. \end{aligned} \quad (42)$$

For the first term on the right-hand side, we obtain as in (38)

$$(\nu \nabla u - \nu_h \nabla \tilde{u}, \nabla(z - I_h z))_\Omega \leq c h_P^{3/2} \left(n_l^{1/2} + 1 \right) \|u\|_{H^3(\Omega_1 \cup \Omega_2)} \|\nu_h^{1/2} \nabla(z - I_h z)\|_{S_h}$$

For the last term, we estimate using (12), (13) and (22)

$$\begin{aligned} \|\nu_h^{1/2} \nabla(z - I_h z)\|_{S_h} &\leq c(\epsilon) \left(n_l^{1/2} h_P^{3/2-\epsilon} + h_P^{3/2} \right) \|z - I_h z\|_{H^2(\Omega_1 \cup \Omega_2)} \\ &\leq c(\epsilon) \left(n_l^{1/2} h_P^{3/2-\epsilon} + h_P^{3/2} \right). \end{aligned}$$

The second term in (40) is easily estimated with the bound for the energy norm error and the interpolation error (22)

$$(\nu_h \nabla(\tilde{u} - u_h), \nabla(z - I_h z))_\Omega \leq c \left(n_l^{\frac{1}{2}} + 1 \right) h_P^3 \|u\|_{H^3(\Omega_1 \cup \Omega_2)}.$$

For the third term in (42), we use the perturbed Galerkin orthogonality (32)

$$\begin{aligned} (\nu \nabla u - \nu_h \nabla u_h, \nabla I_h z)_\Omega &= (f - f_h, I_h z)_{S_h} \\ &\leq \|f_1 - f_2\|_{S_{h,lin}} \|I_h z\|_{S_{h,lin}} + \|f_1 - f_2\|_{S_{h,qu}} \|I_h z\|_{S_{h,qu}}. \end{aligned} \tag{43}$$

For the first part in both terms, we use (12) and (13), respectively

$$\|f_1 - f_2\|_{S_{h,lin}} + \|f_1 - f_2\|_{S_{h,qu}} \leq \left(c(\epsilon) n_l^{\frac{1}{2}} h_P^{\frac{3}{2}-\epsilon} + c h_P^{\frac{3}{2}} \right) \|f\|_{H^1(\Omega_1 \cup \Omega_2)}.$$

For the remaining terms in (43), it is sufficient to consider the smallness of $|S_h|$, a Sobolev imbedding and the continuity of the extension (18)

$$\begin{aligned} \|I_h z\|_{S_{h,lin}} &\leq |S_{h,lin}|^{\frac{1}{2}} \|I_h z\|_{L^\infty(\Omega)} \leq c n_l^{\frac{1}{2}} h_P^{\frac{3}{2}} \|z\|_{L^\infty(\Omega)} \leq c n_l^{\frac{1}{2}} h_P^{\frac{3}{2}} \|z\|_{H^2(\Omega_1 \cup \Omega_2)} \leq c n_l^{\frac{1}{2}} h_P^{\frac{3}{2}} \\ \|I_h z\|_{S_{h,qu}} &\leq |S_{h,qu}|^{\frac{1}{2}} \|I_h z\|_{L^\infty(\Omega)} \leq c h_P^{\frac{3}{2}}. \end{aligned}$$

Altogether this yields the following estimate for the term in (42), which completes the proof of the L^2 -norm estimate

$$(\nu \nabla u - \nu_h \nabla u_h, \nabla z)_\Omega \leq c(\epsilon) \left(n_l h_P^{3-\epsilon} + h_P^3 \right) \|f\|_{H^1(\Omega_1 \cup \Omega_2)}.$$

□

Remark 4. (*Optimality of the energy norm estimate*) The energy norm estimate

$$\|\nu_h^{1/2} \nabla(u - u_h)\|_\Omega = \mathcal{O}(h_P^{\frac{3}{2}}) \tag{44}$$

is optimal, even for a fully quadratic interface approximation ($n_l = 0$). This comes from the interpolation estimate $\|\nabla(u - I_h u)\|$, where the term $\|\nabla(u - \tilde{u})\|_{S_h} = \mathcal{O}(h_P^{3/2})$ needs to be estimated, see Remark 2. One possible remedy, which has been chosen in Theorem 6 is to estimate $\|\nu_h^{1/2} \nabla(\tilde{u} - u_h)\|$. The result is sufficient as a basis for the L^2 -norm estimate.

Another possibility would be to extend the normal and tangential vectors to the whole domain Ω and to derive the following energy-type estimate

$$(\|\nu \partial_n u - \nu_h \partial_n u_h\|_\Omega^2 + \|\nu_h \partial_\tau(u - u_h)\|_\Omega^2)^{\frac{1}{2}} \leq \left(c(\epsilon) n_l^{\frac{1}{2}} h_P^{2-\epsilon} + c_2 h_P^2 \right) \|f\|_{H^1(\Omega_1 \cup \Omega_2)}. \quad (45)$$

(In fact, it would be enough to define the normal and tangential vectors in the interface cells S_T , as $\nu = \nu_h$ everywhere else.) In contrast to $\partial_n u$, the terms $\nu \partial_n u$ and $\partial_\tau u$ are continuous across the interface. This can be used in the energy estimate to show the result (45). As this estimate is slightly more technical, we have decided to restrict ourselves to (30) in this work.

Remark 5. (Constants $c(\epsilon)$) The constants $c(\epsilon) = c(p)$ in Theorem 6 are the constants of the Sobolev imbeddings $H^1(\Omega) \subset L^p(\Omega)$

$$\|u\|_{L^p(\Omega)} \leq c(p) \|u\|_{H^1(\Omega)}$$

for $p < \infty$ with $p \approx \epsilon^{-1}$. This estimate is valid for any fixed $p < \infty$ ($\epsilon > 0$) with an associated constant $c(p)$. The minimizing value ϵ^* of the function $g(\epsilon) := c(\epsilon) h^{-\epsilon}$, for which the estimates in Theorem 6 get optimal, will be analyzed in the numerical examples below.

4 Implementation

The locally modified finite element method is based on a patch-wise parametric approach. Let \mathcal{T}_h be the triangulation. We denote by $P \in \mathcal{T}_h$ the patches, which are quadrilaterals with 25 degrees of freedom. Depending on the location of the interface, we have two kinds of patches:

- If the patch is not cut by the interface, then the patch is split into four quadrilaterals K_1, \dots, K_4 . In this case we take the standard space of piecewise biquadratic functions as follows:

$$\hat{Q} := \{\phi \in C(\hat{P}), \phi|_{\hat{K}_i} \in \text{span}\{1, x, y, x^2, xy, y^2, x^2y, xy^2\}, i = 1, \dots, 4\},$$

where \hat{P} is the reference patch on the unit square $(0, 1)^2$ consisting of the four quadrilaterals $\hat{K}_1, \dots, \hat{K}_4$.

- If the patch is cut by the interface, then the patch is split into eight triangles T_1, \dots, T_8 . Here we define the space of piecewise quadratic functions as follows:

$$\hat{Q}_{mod} := \{\phi \in C(\hat{P}), \phi|_{\hat{T}_i} \in \text{span}\{1, x, y, x^2, xy, y^2\}, i = 1, \dots, 8\},$$

where the reference patch \hat{P} consists of triangles $\hat{T}_1, \dots, \hat{T}_8$.

In both cases, we have locally 25 basis functions in each patch (see Figure 6)

$$Q(P) := \text{span}\{\phi_i\}, \phi_i := \hat{\phi}_i \circ \hat{T}_P^{-1}, i = 1, \dots, 25,$$

where \hat{T}_P is the reference patch map, which is defined in an isoparametric way as follows

$$\hat{T}_P(\hat{x}) := \sum_{j=1}^{25} x_j \hat{\phi}_j. \quad (46)$$

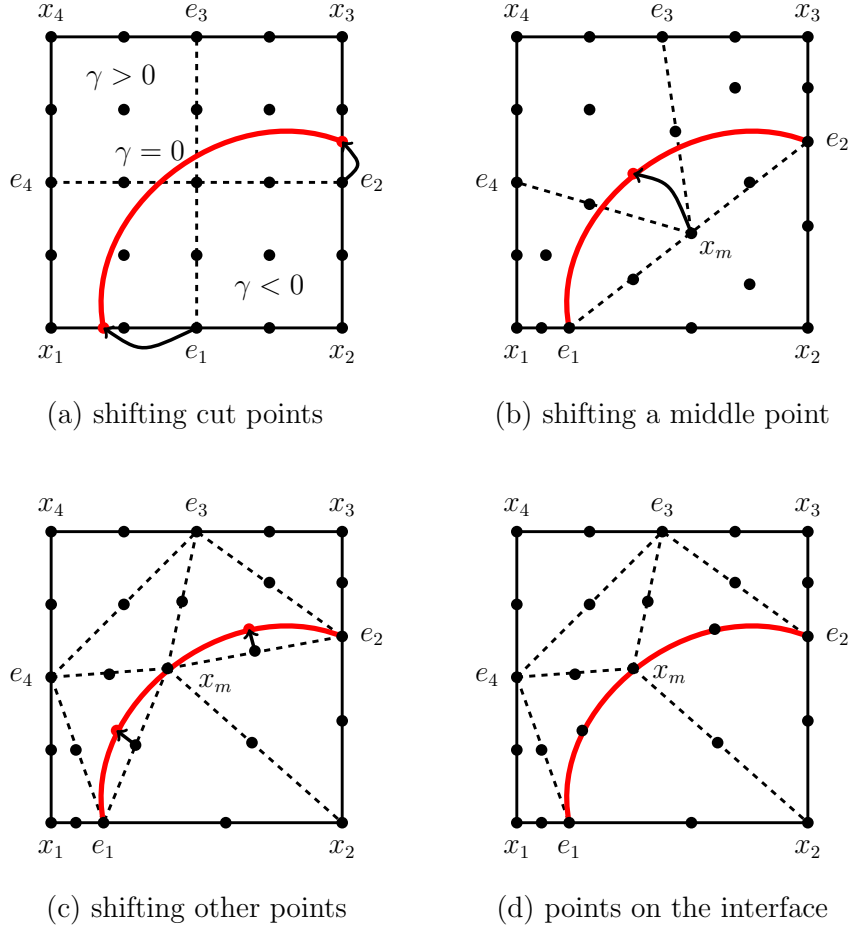


Figure 6. Rearrangement of the Lagrangian points on the interface.

Defining the patch type and movement of mesh nodes We assume that the interface is given as zero set of an implicit level-set function $\gamma(x)$

$$\gamma(x) = 0 \quad \Leftrightarrow \quad x \in \Gamma.$$

The patch type and the edges that are cut can then be easily determined by computing $\gamma(x_i)$ for the exterior vertices x_1, \dots, x_4 , see Figure 6. An edge e is cut, if $\gamma(x_1) \cdot \gamma(x_2) < 0$ for its two end points x_1, x_2 . The intersection of the interface with the edge can be found by applying locally a Newton's method to find the zero r of

$$\gamma(x_1 + r(x_2 - x_1)) = 0, \quad (47)$$

see Figure 6 (a). The edge midpoints e_1 and e_2 will be moved to the respective position $x_1 + r(x_2 - x_1)$. Next, we define a preliminary coordinate for the midpoint of the patch x_m as the midpoint of a segment e_1e_2 , see Figure 6 (b). For a second-order interface approximation, it is necessary to move x_m to the interface Γ in the configurations A to D. We use again Newton's method to move x_m to the interface along a normal line, see Figure 6 (c). Second, we also move the midpoints of the

segments e_1x_m and x_me_2 analogously, see Figure 6 (d). Finally, we need to specify a criteria to ensure that the resulting sub-triangles with curved boundaries fulfill a maximum angle condition. Details are given in the appendix C.

Remark 6. A disadvantage of the modified second order finite element method described above is that the stiffness matrix can be ill-conditioned for certain anisotropies. In particular, the condition number depends not only on the mesh size, but also on how the interface intersects the triangulation (e.g., $s, r \rightarrow 0$). In section 5 we consider two examples, where the condition number of the stiffness matrix is not bounded. For this reason a hierarchical finite element basis was introduced in^[1] for linear the finite elements and it was shown that the stiffness matrix satisfies the usual bound $\mathcal{O}(h_P^{-2})$ with a constant that does not depend on the position of the interface. We extend this approach to the second order finite element method below. We will see that the condition number for a scaled hierarchical basis is reduced significantly, although we can not guarantee the optimal bound for the method presented here.

5 Numerical examples

5.1 Example 1

We consider a square domain $\Omega = (-2, 2)^2$. The domain is split into two domains Ω_1 and Ω_2 by the interface Γ . The interface is defined as $\Gamma\{(x, y) \in \Omega \mid l(x, y) = 0\}$ with the level-set function $l(x, y) = y - 2(x + \delta h)^2 + 0.5$, where $\delta \in [0, 1]$ and h is the mesh size. We take $\nu_1 = 4$ and $\nu_2 = 1$ and choose the exact solution as follows

$$u(x, y) = \begin{cases} \frac{1}{\nu_1} \sin(l), & \text{in } \Omega_1, \\ \frac{1}{\nu_2} \sin(l), & \text{in } \Omega_2, \end{cases}$$

and define a right-hand side $f_i = -\nu_i \Delta u$ and Dirichlet boundary data. We vary $\delta \in [0, 1]$, such that this example includes different configurations with arbitrary anisotropies. The configuration and the exact solution for this example are shown in Figure 7. In this example the interface could be resolved with second order on all

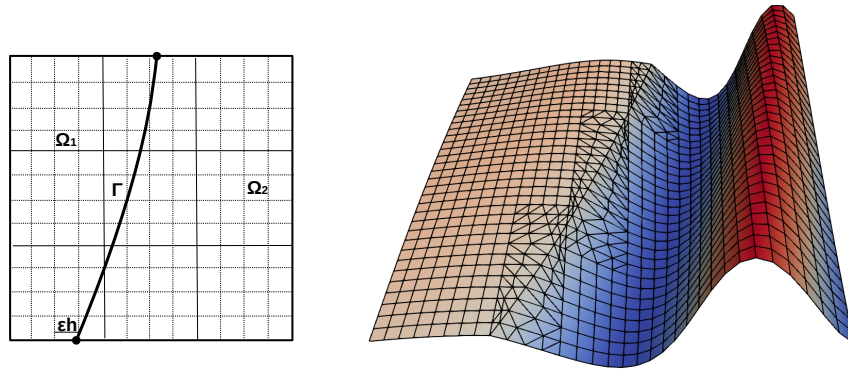


Figure 7. Left: Configuration of the test problem. Right: Sketch of the exact solution

meshes ($n_l = 0$). We will show the modified energy norm error ($\|\nu_h^{1/2} \nabla(\tilde{u} - u_h)\|$) and the L^2 - norm error. We do not show the energy norm error $\|\nabla(u - u_h)\|_\Omega$ here, as its evaluation would require the construction of complex quadrature formulae, due to the discontinuities of ∇u across Γ and ∇u_h across Γ_h . An accurate quadrature

formula would need to resolve both the discrete interface Γ_h and the continuous interface Γ . Inaccurate formulas, such as a summed midpoint rule, automatically lead to an additional error of order $\mathcal{O}(h_P^{3/2})$. The evaluation of the modified energy norm is much easier, as both quantities \tilde{u} and u_h are regular within a cell T .

Table 1 shows the errors as well as estimated convergence orders on several levels of global mesh refinement for the fixed parameter $\delta = 0$. According to the a priori error estimate in Theorem 6, we observe fully quadratic convergence in the modified energy norm and fully cubic convergence in the L^2 - norm. We plot the modified

h	L^2 - error	EOC	energy error	EOC
1/32	$1.74 \cdot 10^{-4}$	-	$2.08 \cdot 10^{-2}$	-
1/64	$2.13 \cdot 10^{-5}$	3.023	$5.22 \cdot 10^{-3}$	1.998
1/128	$2.65 \cdot 10^{-6}$	3.006	$1.31 \cdot 10^{-3}$	1.999
1/256	$3.31 \cdot 10^{-7}$	3.004	$3.26 \cdot 10^{-4}$	2.000

Table 1. Errors in the L^2 - norm and the modified energy norm, including an estimated order of convergence which is computed from two consecutive values in each row for Example 1 and $\delta = 0$.

energy norm error and the L^2 - norm error for $\delta \in [0, 1]$ on several levels of global mesh refinement in Figure 8 and observe that the error is bounded independently of δ .

In Figure 9, we show how the condition number depends on the parameter $\delta \in [0, 1]$ by moving the interface. We get the largest condition numbers at $\delta = 0.84$. Furthermore, we show a zoom-in of the numbers for $\delta \in [0.83; 0.85]$ in Figure 9, right. We see that the condition number for the scaled hierarchical basis is reduced by a factor of 100, but is not necessarily bounded for arbitrary anisotropies.

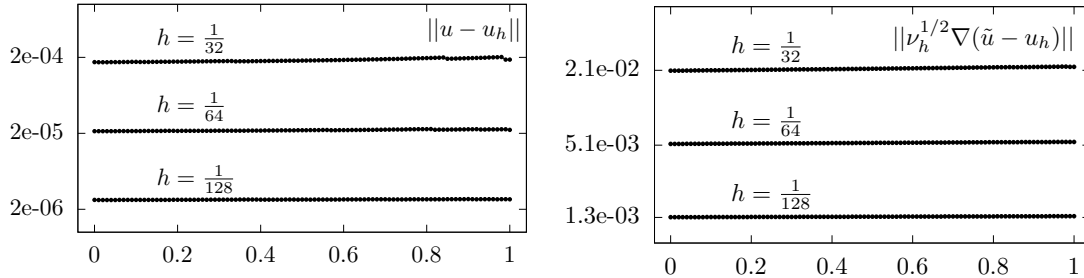


Figure 8. L^2 - norm and modified energy norm errors for Example 1 with $x = 1.0 + \delta h$ and $\delta \in [0, 1]$.

5.2 Example 2

We consider a square domain $\Omega = (-2, 2)^2$ that is split into a ball $\Omega_1 = B_r(x_0, y_0)$ with $r = 0.3$ and $(x_0, y_0) = (1 + \delta h, 1.2)$, where $\delta \in [0, 1]$, and $\Omega_2 = \Omega \setminus \bar{\Omega}_1$. We take the exact solution as in example 1, with the level set function replaced by $l(x, y) = (x - x_0)^2 + (y - y_0)^2 - r^2$. In Figure 10 we show the configuration and the exact solution of this example. For different $\delta \in [0, 1]$, this example includes all above discussed configurations with different anisotropies.

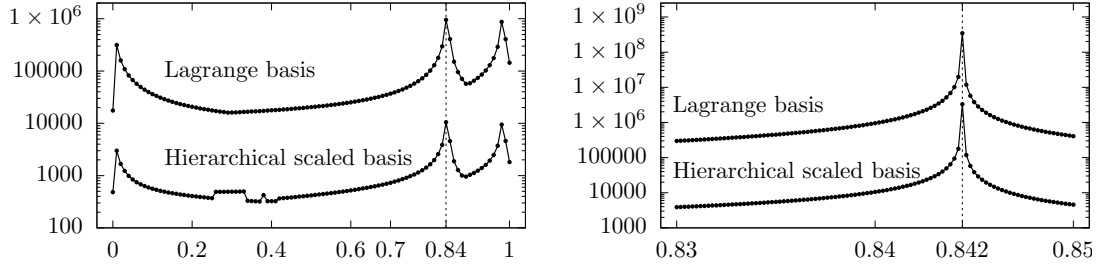


Figure 9. Condition number of the stiffness matrix depending on the position of the interface δ . Comparison of the standard Lagrangian basis and a scaled hierarchical basis for $h = 1/32$. *Left:* $\delta \in [0, 1]$. *Right:* Zoom-in for $\delta \in [0.83, 0.85]$.

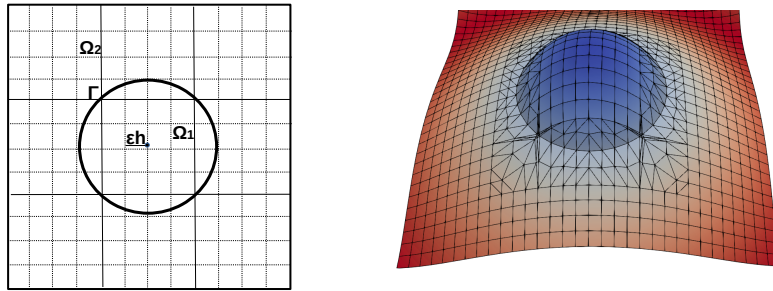


Figure 10. *Left:* Configuration of the test problem. *Right:* Sketch of the exact solution

The L^2 -norm and the modified energy norm errors are shown in Figure 11 for $\delta \in [0, 1]$ on several levels of global mesh refinement. We observe convergence in both norms for $\delta > 0$. The errors vary slightly depending on δ . Its magnitude depends mainly on the number of linearly approximated elements (n_l): We have $n_l = 0$ for $\delta = 0$ on all mesh levels, while $n_l > 0$ for all other values of δ . We observe that the errors increase from $\delta = 0$ to $\delta = 0.01$, as n_l increases from 0 to 8. Moreover, the number of linearly approximated elements increases for $h = 1/64$ once more, from $n_l = 8$ to $n_l = 16$ in the range $\delta \in [0.74, 0.81]$. Again, we observe a slight increase in the magnitude of the error within this range. This indicates that the constant $c(\epsilon)$ in front of the linearly approximated part is larger than the constant c_2 arising from the quadratically approximated elements.

Table 2, Table 3 and Table 4 show the L^2 -norm and the modified energy norm errors obtained on several levels of global mesh refinement for the fixed positions $x_0 = 1.0 + \frac{\delta_0}{64}$ of the midpoint, with $\delta_0 \in \{0, 0.01, 0.8\}$, which results in three different cases ($n_l = 0, n_l = 8$ and $n_l = 16$) for $h = 1/64$.

In Table 2 ($\delta_0 = 0$) we observe fully quadratic (resp. cubic convergence) in the modified energy norm (resp. the L^2 -norm) as predicted in Theorem 6, as no linearly approximated elements are present. This changes slightly for the other values of δ_0 , see Table 3 and Table 4.

In Table 3 ($\delta_0 = 0.01$), we see that 8 linearly approximated elements were required on all mesh levels. The convergence order in the modified energy norm seems to be fully quadratic, while in the L^2 -norm error the reduced convergence order $3 - \epsilon$, predicted by Theorem 6, is visible. The optimal value ϵ^* (cf. Remark 5) seems to lie around $\epsilon^* \approx 0.08$ in this example, which results in a convergence order around 2.92.

For $\delta_0 = 0.8$ the number n_l increases from 8 to 16 between the coarsest and the

second-coarsest refinement level and stays constant from then on. This is again reflected in the magnitude of the error: The reduction factor between the coarsest mesh levels lies below 4 in the modified energy, and below 8 in the L^2 -norm error, which shows again that the constant $c(\epsilon)$ in front of the linearly approximated part is larger than the constant c_2 in front of the quadratic counterpart. On the remaining mesh levels, the estimated orders of convergence are again fully quadratic in the modified energy norm and $3 - \epsilon$ in the L^2 -norm. We note that both for fixed $n_l = 8$ and $n_l = 16$ the convergence orders are in agreement with Theorem 6.

For $\delta_0 = 0.8$ and $h_P = \frac{1}{32}$, we show the resulting finite element mesh in Figure 12, where in 8 of the 18 patches, which are cut by the interface, a linear approximation was required, including a zoom around one linearly approximated patch on the right.

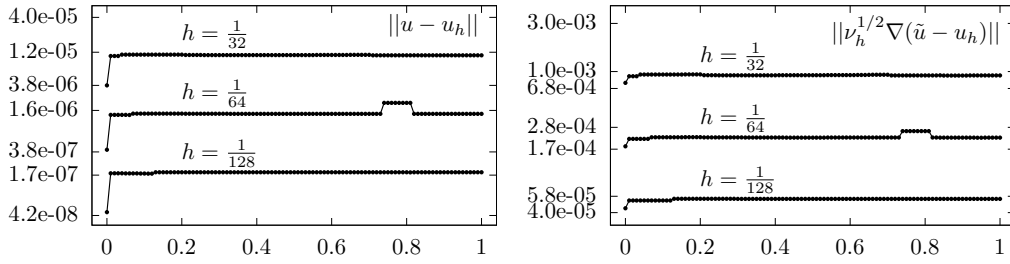


Figure 11. L^2 - norm and modified energy - norm errors depending on the position $x = 1.0 + \delta h$ of the midpoint with $\delta \in [0, 1]$.

h	L^2 - error	EOC	energy error	EOC
1/32	$3.44 \cdot 10^{-6}$	-	$4.36 \cdot 10^{-4}$	-
1/64	$3.85 \cdot 10^{-7}$	3.159	$9.69 \cdot 10^{-5}$	2.170
1/128	$4.56 \cdot 10^{-8}$	3.078	$2.28 \cdot 10^{-5}$	2.085
1/256	$5.54 \cdot 10^{-9}$	3.040	$5.52 \cdot 10^{-6}$	2.048

Table 2. L^2 -norm and modified energy norm errors, and convergence order for $\delta_0 = 0$ ($n_l = 0$).

h	L^2 - error	EOC	energy error	EOC	PN	n_l
1/32	$1.05 \cdot 10^{-5}$	-	$9.00 \cdot 10^{-4}$	-	18	8
1/64	$1.37 \cdot 10^{-6}$	2.943	$2.15 \cdot 10^{-4}$	2.066	36	8
1/128	$1.81 \cdot 10^{-7}$	2.920	$5.27 \cdot 10^{-5}$	2.028	76	8
1/256	$2.39 \cdot 10^{-8}$	2.921	$1.30 \cdot 10^{-5}$	2.015	154	8

Table 3. L^2 - and modified energy - norm errors for $\delta_0 = 0.01$, including estimated convergence orders obtained from two consecutive values. PN denotes the number of patches which are cut by the interface and n_l the number of the linear approximated elements.

In Figure 13 we show how the condition numbers depend on the parameter $\delta \in [0, 1]$ when moving the interface. We get the largest condition numbers at $\delta \approx 0.04$ for $h = 1/32$ and at $\delta \approx 0.07$ for $h = 1/64$, respectively. The condition numbers are

h	L^2 - error	EOC	energy error	EOC	PN	n_l
1/32	$1.09 \cdot 10^{-5}$	-	$9.19 \cdot 10^{-4}$	-	18	8
1/64	$2.07 \cdot 10^{-6}$	2.390	$2.57 \cdot 10^{-4}$	1.839	36	16
1/128	$2.73 \cdot 10^{-7}$	2.924	$6.35 \cdot 10^{-5}$	2.016	76	16
1/256	$3.59 \cdot 10^{-8}$	2.927	$1.58 \cdot 10^{-5}$	2.007	152	16

Table 4. L^2 and modified energy - norm errors, including an estimated convergence order for $\delta = 0.8$.

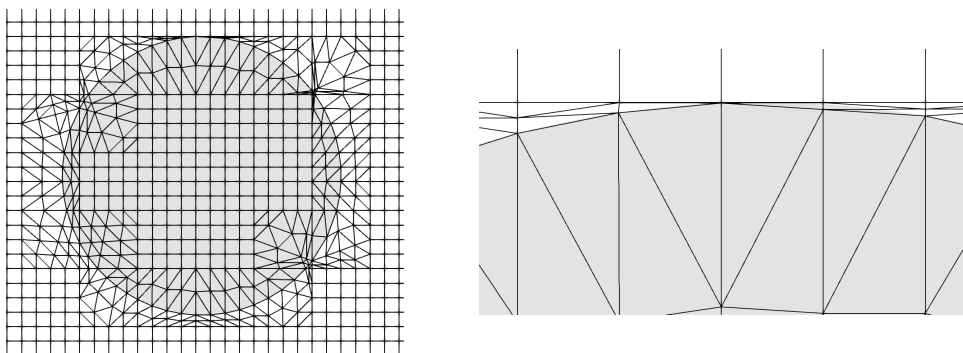


Figure 12. Left: Illustration of the sub-elements for $h = 1/32$ and $\delta = 0.8$. Right: Zoom of the upper part with linearly approximated elements (top right).

again reduced by a factor of approx. 100 for the scaled hierarchical basis compared to the standard Lagrangian basis.

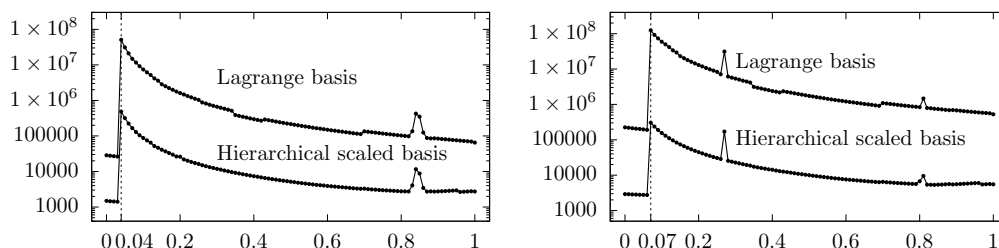


Figure 13. Condition number of the stiffness matrix depending on the displacement of the circle. Comparison of the Lagrange and hierarchical scaled basis for $h = 1/32$ (left) and $h = 1/64$ (right).

6 Conclusion

We have presented an extension of the locally modified finite element method for interface problem that was introduced in^[1], to second order. We were able to show optimal-order error estimates of order $3 - \epsilon$ in the L^2 -norm and $2 - \epsilon$ in a modified energy norm, which considers the different positions of discrete and continuous interface. In the standard H^1 -norm the convergence order is reduced to 1.5, due to the mismatch of continuous and discrete interface. Finally, we have presented different numerical examples that illustrate the convergence behaviour and the performance of the method. In future, we plan to apply the discretisation to *inf-sup* stable elements

for the discretisation of interface problems including the Stokes- and Navier-Stokes equations.

Appendix A: Linear interface approximation

We distinguish between the following five cases, see Figure 2

- Configuration A: The patch is cut in two opposite nodes.
- Configuration B: The patch is cut at the interior of one edge and in one node.
- Configuration C: The patch is cut at the interior of two opposite edges.
- Configuration D: The patch is cut at the interior of two adjacent edges with $r \in (0, \frac{1}{2})$, $s \in (\frac{1}{2}, 1)$.
- Configuration E: The patch is cut at the interior of two adjacent edges with
 - $r \in (0, 1)$ and $s \in (0, \frac{1}{2})$
 - $r \in (\frac{1}{2}, 1)$ and $s \in (0, 1)$

The subdivisions can be anisotropic with the parameters $r, s \in (0, 1)$ in the configurations B , C , D and E . These parameters describe the relative position of the intersection points with the interface on the edges. We denote by $e_i \in \mathbb{R}$, $i = 1, 2, 3, 4$, the vertices on the edge. When the interface intersects an edge, then we move the corresponding point e_i , $i = 1, \dots, 4$ on the intersected edge to the point of the intersection (see Figure 2). If an edge is not intersected by the interface then we take e_i as midpoint of this edge. By $x_m \in \mathbb{R}^2$ we denote the midpoint of the patch, which has different positions depending on the configurations. We choose the midpoint as the intersection of the line connecting e_1 and e_3 with the line connecting e_2 and e_4 for the configurations A , C and E . For the configuration B we choose the midpoint as the intersection of the line connecting e_1 and e_3 with the line connecting x_1 and e_2 . The midpoint for the configuration D can be chosen as the midpoint of the line segment e_1e_2 .

The patch in all configurations is split into four quadrilaterals. Each quadrilateral has at least one right angle. Depending on the configurations we will get different types of the quadrilaterals. In configuration A we have a square and in the other configurations we get different types of the quadrilaterals. In the configurations B and C we get a right-angled trapezoid. In the configuration D we have a quadrilateral with one large interior angle which is equal to 180° and in the configuration E we have quadrilaterals with one or two large interior angles between $(90^\circ, 180^\circ)$.

Therefore, we distinguish two different types for a quadrilateral with one right angle:

1. The quadrilateral has one interior largest angle equal to 180° ,
2. The quadrilateral has one or two interior largest angles between 90° and 180° .

We split all types of quadrilaterals into two triangles by splitting the largest interior angle of the quadrilateral.

Appendix B: Proof of Lemma 1

Proof. First, the patch is split into four sub-quadrilaterals K_1, \dots, K_4 , each of which is then split into two triangles. If we can show that all angles of the quadrilaterals are bounded by 135° , this applies for the sub-triangles as well. Moreover, if the splitting

into triangles in K_i for some $i = 1, \dots, 4$ is not determined by the interface position, we split in such a way that the largest angle of K_i is divided. In this case the bound for the maximum angles of the sub-triangles can be further improved.

We consider now the configurations A,B,C,D,E shown in Figures 2 separately. In all cases the angles at the vertices $x_i, i = 1, \dots, 4$ are exactly 90° and the angles at the edge midpoints $e_i, i = 1, \dots, 4$ lie between 45° and 135° (Note that this bound is not sharp, if we divide in an optimal way into sub-triangles).

In the configuration *A* we have two squares and four right-angled triangles. This case is obvious and the maximum angle of the sub-triangles is 90° .

In configuration *B* and *C* each quadrilateral $K_i (i = 1, \dots, 4)$ has two right angles, as the positions of e_1 and e_3 , or e_2 and e_4 , respectively, are fixed. Let us consider exemplarily the configuration shown in Figures 2(b). As mentioned above, the angles in e_2 and e_4 lie between 45° and 135° . By symmetry the angles around x_m are exactly the same. Therefore, in both configurations all angles of the sub-triangles lie below 135° .

In configuration *D*, we get one degenerate quadrilateral K_2 with a maximum angle of 180° . As this angle is divided by connecting x_m and x_2 we have the following bounds for the triangles of K_2

$$\begin{aligned} \cos(\angle e_1 x_m x_2) &= \frac{(e_1 - x_m) \cdot (x_2 - x_m)}{|e_1 - x_m| \cdot |x_2 - x_m|} = \frac{((r-1), -s) \cdot ((1-r), -s)}{(1-r)^2 + s^2} \\ &= \frac{-(1-r)^2 + s^2}{(1-r)^2 + s^2} \in \left(-\frac{3}{5}, \frac{3}{5}\right). \end{aligned}$$

such that $\angle e_1 x_m x_2 \in (53^\circ, 127^\circ)$. The other angles in x_m are bounded above by 90° . The angles in e_1, \dots, e_4 are again bounded by 135° .

In configuration *E*, the angles in e_1, \dots, e_4 are all between 63° and 117° . A bound on the angles of the quadrilaterals at x_m is therefore given by $360^\circ - 2 \cdot 63^\circ - 90^\circ = 144^\circ$. This maximum is attained for $r \rightarrow 1, s \rightarrow 0$ (cf. Figure 2 (f)). The bound is further improved, as in K_1, K_2 and K_3 the largest angles are divided when splitting into sub-triangles, resulting in angles below 90° . For the angle of T_1 at x_m we have

$$\begin{aligned} \cos(\angle e_1 x_m e_2) &= \frac{(e_1 - e_3) \cdot (e_2 - e_4)}{|e_1 - e_3| \cdot |e_2 - e_4|} = \frac{(r-1/2, -1) \cdot (1, s-1/2)}{\sqrt{1+(r-1/2)^2} \cdot \sqrt{1+(s-1/2)^2}} \\ &= \frac{r-s}{\sqrt{1+(r-1/2)^2} \cdot \sqrt{1+(s-1/2)^2}} \in \left(-\frac{1}{\sqrt{5}}, \frac{4}{5}\right) \end{aligned}$$

such that $\angle e_1 x_m e_2 \in (36^\circ, 117^\circ)$. □

Appendix C: Quadratic interface approximation

For the elements with curved boundaries we need to ensure that all elements are allowed in the sense of Assumption 1 (see also Figure 1) and that the maximum angle condition shown above remains valid. As described in Section 4, we move certain points to the interface in order to obtain a second-order interface approximation. This is possible if the following criteria are satisfied. Otherwise, we leave them in their original positions and obtain a first-order interface approximation in the respective element. By α_Δ we denote the largest angle in a triangle.

In the first step, we move the midpoint of the patch. If this is possible, we shift the other corresponding points in a second step (if possible). We use the following criteria for each configuration.

First step: Move the midpoints

- **Configuration A:** the midpoint of the patch can be moved along the normal line \mathbf{n} (see Figure 2a) if $\alpha_\Delta \leq \alpha_{max} < 180^\circ$.
- **Configuration B:** the midpoint of the patch can be moved along the line segment e_1e_3 , if the relative length $d = \frac{|e_1 - x_m|}{|e_2 - e_1|}$ of the line e_1x_m (see Figure 2b) satisfies $\epsilon < d < 1 - \epsilon$ and $\alpha_\Delta \leq \alpha_{max} < 180^\circ$.
- **Configuration C:** the midpoint of the patch can be moved along the line segment e_2e_4 , if the parameter d (see Figure 2c) satisfies $\epsilon < d < 1 - \epsilon$.
- **Configuration D:** the midpoint of the patch can be moved along the normal line \mathbf{n} (see Figure 2d) if $\alpha_\Delta \leq \alpha_{max} < 180^\circ$.
- **Configuration E:** in this configuration we do not need to move the midpoint of the patch (see Figures 2e), and 2f).

Second step: Move other points

- In the second step, we investigate the other two points that need to be moved in order to obtain a second-order interface approximation. These are the points between the midpoint of the patch and the points where exterior edges are intersected. In all configurations, we obtain triangles with one curved edge (see Figure 3). It can happen that this curved edge intersects other edges of the element T . Thus, we shift the corresponding points along the normal line to the interface, if and only if the curved edge of the triangle does not cut any other edges and $\alpha_\Delta \leq \alpha_{max} < 180^\circ$.

References

- [1] S. Frei and T. Richter, “A locally modified parametric finite element method for interface problems,” *SIAM Journal on Numerical Analysis*, vol. 52, pp. 2315–2334, 2014.
- [2] T. Richter, *Fluid Structure Interactions: Models, Analysis and Finite Elements*. Springer, 2017.
- [3] S. Frei, “Eulerian finite element methods for interface problems and fluid-structure interactions,” *PhD thesis, Heidelberg University*, <http://www.ub.uni-heidelberg.de/archiv/21590>, 2016.
- [4] I. Babuška, “The finite element method for elliptic equations with discontinuous coefficients,” *Computing*, vol. 5, pp. 207–213, 1970.
- [5] S. Frei, T. Richter, and T. Wick, “Long-term simulation of large deformation, mechano-chemical fluid-structure interactions in {ALE} and fully eulerian coordinates,” *Journal of Computational Physics*, vol. 321, pp. 874 – 891, 2016.
- [6] S. Frei, T. Richter, and T. Wick, “Eulerian techniques for fluid-structure interactions: Part I—Modeling and simulation,” in *Numerical Mathematics and Advanced Applications-ENUMATH 2013*, pp. 745–753, Springer, 2015.

- [7] S. Frei, T. Richter, and T. Wick, “Eulerian techniques for fluid-structure interactions: Part II–Applications,” in *Numerical Mathematics and Advanced Applications-ENUMATH 2013*, pp. 755–762, Springer, 2015.
- [8] U. Langer and H. Yang, “Numerical simulation of parabolic moving and growing interface problems using small mesh deformation,” *Bericht-Nr. 2015-16; Johann Radon Institute for Computational and Applied Mathematics*.
- [9] E. Burman, M. A. Fernández, and S. Frei, “A nitsche-based formulation for fluid-structure interactions with contact,” *ESAIM: M2AN*, vol. 54, no. 2, pp. 531–564, 2020.
- [10] S. Frei and T. Richter, “An accurate Eulerian approach for fluid-structure interactions,” in *Fluid-Structure Interaction: Modeling, Adaptive Discretization and Solvers* (S. Frei, B. Holm, T. Richter, T. Wick, and H. Yang, eds.), Radon Series on Computational and Applied Mathematics, pp. 69–126, Walter de Gruyter, Berlin, 2017.
- [11] J. Hoffman, B. Holm, and T. Richter, “The locally adapted parametric finite element method for interface problems on triangular meshes,” in *Fluid-Structure Interaction: Modeling, Adaptive Discretization and Solvers* (S. Frei, B. Holm, T. Richter, T. Wick, and H. Yang, eds.), Radon Ser Comput Appl Math, pp. 41–68, de Gruyter, 2017.
- [12] P. Gangl, “A local mesh modification strategy for interface problems with application to shape and topology optimization,” in *Scientific Computing in Electrical Engineering*, pp. 147–155, Springer, Cham, 2018.
- [13] S. Frei, “An edge-based pressure stabilization technique for finite elements on arbitrarily anisotropic meshes,” *Int J Numer Methods Fluids*, vol. 89, no. 10, pp. 407–429, 2019.
- [14] S. Frei and T. Richter, “A second order time-stepping scheme for parabolic interface problems with moving interfaces,” *ESAIM: Mathematical Modelling and Numerical Analysis*, vol. 51, no. 4, pp. 1539–1560, 2017.
- [15] S. Frei, T. Richter, and T. Wick, “On the implementation of a locally modified finite element method for interface problems in deal.ii,” *arXiv e-print 1806.00999*, 2018.
- [16] S. Frei, T. Richter, and T. Wick, “An implementation of a locally modified finite element method for interface problems in deal.II,” *Zenodo*, 2018. <https://doi.org/10.5281/zenodo.1457758>.
- [17] U. Langer and H. Yang, “Numerical simulation of parabolic moving and growing interface problems using small mesh deformation,” 2015.
- [18] S. Hoöllbacher and G. Wittum, “A sharp interface method using enriched finite elements for elliptic interface problems.”.
- [19] A. Vogel, S. Reiter, M. Rupp, A. Nägel, and G. Wittum, “Ug 4: A novel flexible software system for simulating pde based models on high performance computers,” *Comput Visual Sci*, vol. 16, no. 4, pp. 165–179, 2013.

- [20] N. Moës, J. Dolbow, and T. Belytschko, “A finite element method for crack growth without remeshing,” *Int J Numer Methods Eng*, vol. 46, pp. 131–150, 1999.
- [21] I. Babuška, U. Banarjee, and J. E. Osborn, “Generalized finite element methods: Main ideas, results, and perspective,” *Int J Comput Methods*, vol. 1, pp. 67–103, 2004.
- [22] A. Hansbo and P. Hansbo, “An unfitted finite element method, based on Nitsche’s method, for elliptic interface problems,” vol. 191, no. 47-48, pp. 5537–5552, 2002.
- [23] E. Burman and P. Hansbo, “Fictitious domain finite element methods using cut elements: Ii. a stabilized nitsche method,” *Applied Numerical Mathematics*, vol. 62, no. 4, pp. 328–341, 2012.
- [24] C. Lehrenfeld, “High order unfitted finite element methods on level set domains using isoparametric mappings,” *Comput Methods Appl Mech Eng*, vol. 300, pp. 716 – 733, 2016.
- [25] C. Lehrenfeld and A. Reusken, “Analysis of a high order unfitted finite element method for an elliptic interface problem,” *IMA J. Numer. Anal.*, vol. 38, pp. 1351–1387, 2018.
- [26] C. Lehrenfeld and A. Reusken, “ L^2 -estimates for a high order unfitted finite element method for elliptic interface problems,” *Journal of Numerical Mathematics*, vol. 00, pp. –, 2018. first online.
- [27] I. Babuška, “The finite element method for elliptic equations with discontinuous coefficients,” *Computing*, vol. 5, pp. 207–213, 1970.
- [28] S. Basting and R. Prignitz, “An interface-fitted subspace projection method for finite element simulations of particulate flows,” *Comput. Methods Appl. Mech. Engrg.*, vol. 267, pp. 133–149, 2013.
- [29] J. Bramble and J. King, “A finite element method for interface problems in domains with smooth boundaries and interfaces,” *Adv Comput Math*, vol. 6, pp. 109–138, 1996.
- [30] M. Feistauer and V. Sobotíková, “Finite element approximation of nonlinear problems with discontinuous coefficients,” vol. 24, pp. 457–500, 1990.
- [31] A. Ženíšek, “The finite element method for nonlinear elliptic equations with discontinuous coefficients,” vol. 58, pp. 51–77, 1990.
- [32] C. Börgers, “A triangulation algorithm for fast elliptic solvers based on domain imbedding,” vol. 27, pp. 1187–1196, 1990.
- [33] H. Xie, K. Ito, Z.-L. Li, and J. Toivanen, “A finite element method for interface problems with locally modified triangulation,” *Contemporary Mathematics*, vol. 466, pp. 179–190, 2008.

- [34] X. Fang, “An isoparametric finite element method for elliptic interface problems with nonhomogeneous jump conditions,” *WSEAS Transactions on Mathematics*, vol. 12, 2013.
- [35] J. Wloka, *Partielle Differentialgleichungen*. Teubner, Stuttgart, 1982.